A Nonlinear Robust Controller Design for Path Following of Intelligent Electrical Vehicle

Kada Akermi*, Boudjemaa Boudaa, Samira Chouraqui***

* *Department of Computer Science, University of Science and Technology "Mohamed Boudiaf" USTO Oran Oran BP1505 Algeria (Corresponding author, e-mail: kada.akermi@univ-usto.dz, samira.chouraqui@univ-usto.dz).*
*** Computer Science Department, University of Tiaret, Tiaret, Algeria*
LabRI-SBA Lab., Ecole Superieure en Informatique, Sidi Bel Abbes, Algeria
(e-mail: boudjemaa.boudaa@univ-tiaret.dz)

Abstract: This paper investigates the lateral control of autonomous electrical vehicles; the objective is to minimize the lateral offset with respect to a given reference path. It presents the design and the validation of a new robust and intelligent control strategy using novel sliding mode control (SMC) considering the uncertainties, tires nonlinearities, parametric variations and mismatched disturbances that are encountered in the driving applications. The molded SMC is based on an improved disturbance observer (DOB), a fuzzy system (FS), and a double reaching law. Compared to the existing methods in the literature, the proposed controller behaves adaptively and intelligently with the perturbations encountered. Also, it guarantees vehicle safety and stability on slippery roads while overcoming all the limitations of conventional SMC. The system's stability has been proven using the Lyapunov stability theorem, and simulation results have been validated across extensive scenarios under extreme driving conditions. Compared to the results of conventional SMC and SMC based on the super-twisting algorithm, the proposed controller has demonstrated its superiority.

Keywords: Electrical vehicle, Autonomous vehicle, Path following, Sliding mode control, Fuzzy system, Double reaching law.

1. INTRODUCTION

In recent years, there has been significant progress in intelligent vehicles from the perspective of mobility, safety, and efficiency, leading to many advances in Intelligent Transportation Systems (ITS). Despite these advances, in 2023, 1,354,840 road users died, and as of June 2024[1], there have already been over 647,698 deaths despite efforts made by preventive policies[2]. One of the primary causes of accidents is lateral offset during high-speed travel, particularly when the vehicle navigates a sharp turn.

Autonomous vehicles are one of the best solutions for transforming the conventional transportation system, improving safety, comfort, and stability. Recently, the field of autonomous vehicles has attracted great attention, with many research projects being devoted to this area. Examples include Google's self-driving initiative, which began as R&D in 2009 and evolved into Waymo (Way Forward In Mobile) in 2016. Additionally, notable recent projects include Tesla's Autopilot, introduced in 2014, which is continuously evolving with regular updates to enhance driver assistance and autonomous driving capabilities; Zoox by Amazon, acquired in 2020, which focuses on developing fully autonomous vehicles for the robotaxi market; May Mobility, which has been developing autonomous vehicles for urban areas since 2019 and has provided over 320,000 public rides; AEye, which went public in 2021 and specializes in high-performance lidar technology for autonomous driving; Teleo, which debuted its autonomous materials hauling technology in December 2023, focusing on construction automation; and Hexagon, which released its new iCON 120 machine smart antenna in 2024, advancing machine control capabilities for autonomous construction vehicles.

One of the most fundamental issues for autonomous vehicle motion is lateral control, which aims to guide vehicles along the reference path and reduce the lateral offset to zero while ensuring vehicle safety and stability. Various approaches have been proposed in the literature to address lateral control. For instance, an event-triggered adaptive fuzzy control method is used to manage lateral motion control in (Zhang et al., 2023). In (Nguyenet al., 2022), a Takagi-Sugeno (TS) fuzzy control approach combined with a lateral velocity observer is employed for vehicle lateral motion control. Additionally, (Chen et al., 2024) present an H∞ Fault-Tolerant Observer-Based PID designed for the trajectory tracking of autonomous vehicles. Model Predictive Control (MPC) is commonly utilized for autonomous vehicle path following (Cheng et al., 2020; Liang et al., 2021; Muraleedharan et al., 2022; Lukassek et al., 2024; Pyun et al., 2024) . In (Jin et al., 2024), the authors propose a model predictive control (MPC) approach combined with a physics-informed neural network (PINN) model to tackle intricate trajectory tracking tasks effectively. A Fast Iterative MPC (FI-MPC) framework is introduced for path-following control of autonomous vehicles in (Meng et al., 2024). However, while MPC controllers provide acceptable

[1] https://www.who.int/news-room/fact-sheets/detail/road-traffic-injuries
[2] https://extranet.who.int/roadsafety/death-on-the-roads/

results, their computation time remains a significant drawback. Other significant contributions in this area include the adoption of the Udwadia-Kalaba method for path-following control of autonomous vehicles as detailed in (Sun et al., 2018). The sliding mode controller (SMC) is another commonly used method for motion control in autonomous vehicles. For example, (Fu et al., 2023) designs an SMC combined with the MIT adaptive law to enhance lateral stability, while (Yang et al., 2024) implements a super-twisting sliding mode control with an anti-peaking extended state observer for path-tracking control. Second-order sliding mode control is also utilized in (Chen et al., 2020; Tagn et al., 2016). The integral sliding mode control strategy is typically applied to path-following control, as seen in (Hu et al., 2018; Xu et al., 2018).

The previous controllers proposed for vehicle lateral control struggled to handle uncertainties, high levels of mismatched disturbances, and did not consider variations in parameters such as speed, nor did they enhance the transient performance of the closed-loop system. An initial study related to the SMC controller was introduced in (Akermi et al., 2018), where gain scheduling with a fuzzy system (FS), radial basis function neural networks (RBFNN), and a disturbance observer (DOB) were utilized. To enhance the performance of this controller and overcome the cited drawbacks, the present paper proposes a novel SMC controller for the path-following control of autonomous vehicles. This controller is based on an improved disturbance observer (DOB), a fuzzy system (FS), and a double reaching law. The advantage of this new controller over the one developed in (Akermi et al., 2018) lies in its effective estimation of mismatched disturbances through an enhanced disturbance observer. Additionally, the integration of SMC with the double reaching law offers complementary control, improving the handling of parameter variations and significantly enhancing vehicle safety in critical situations like collision avoidance. The main contributions of this work can be cited as follows:

1. Design of an improved disturbance observer based on a fuzzy system (DOB-FS) to deal with mismatched disturbances, ensuring accurate estimation of the disturbances and maintaining transient performance.
2. Design of a novel robust SMC controller based on the improved disturbance observer, a fuzzy system, and a double reaching law, considering system uncertainties, mismatched disturbances, tire nonlinearities, varying path curvature/speed, and the state of the vehicle/environment. Additionally, the stability of the closed-loop system is proved using the Lyapunov stability theorem.
3. A comparative simulation was conducted by applying both the conventional SMC and the SMC based on the super-twisting algorithm for path-following control.

The remainder of this paper is organized as follows. Section 2 describes the development of our new SMC controller and the use of the Lyapunov stability theorem to prove the global stability of the closed-loop system. Section 3 is devoted to the application of the proposed SMC controller to the lateral control of the autonomous vehicle, including the modeling of the vehicle's lateral dynamics. In the same section, the conventional SMC and SMC Super-twisting are applied to the lateral control to highlight the effectiveness of the proposed controller. Simulation results and comparisons are presented in Section 4. Finally, Section 5 concludes this work by indicating potential future research directions.

2. CONTROLLER DESIGN

This section details the development of our proposed controller by first presenting the fundamental concepts of the disturbance observer, fuzzy system and double hyperbolic reaching law. Then, showcasing the controller design and stability analysis while taking into account uncertainties, mismatched disturbances, and variations in system characteristics.

Given the system that includes uncertainties and mismatched disturbances, as described by

$$\begin{cases} \dot{x} = f(x) + g_1(x)u + g_2 d, \\ y = x_1 \end{cases} \tag{1}$$

where $x = [x_1, x_2]^T$, $f(x) = [x_2, a(x)]^{\mathrm{T}}$, $g_1 = [0, b(x)]^{\mathrm{T}}$, $g_2 = [1, 0]^{\mathrm{T}}$, the state vector is denoted by $[x_1, x_2]$, a and b are two nonlinear uncertain functions. The control input is represented by u, while $d(t)$ signifies the mismatched disturbance, and y indicates the output.

Assumption 1: The mismatched disturbance $d(t)$ is bounded and described by $d^* = \sup_{t>0} |d(t)|$.

2.1 A Disturbance Observer (DOB)

With the high demands on robustness and precision control, mismatched disturbances such as modeling errors and the effects of wind on the vehicle can negatively impact control performance and system stability. In this study, the Disturbance Observer (DOB) is utilized to estimate the mismatched disturbances for this purpose and then considered the estimated disturbances in the control action. To increase the accuracy of the disturbance estimation, an improved disturbance observer based on the equations of the standard DOB introduced and depicted by (Chen, 2003; Yang et al., 2013) is proposed to estimate the uncertain functions using a fuzzy System. The equations of this improved disturbance observer are presented in below:

$$\begin{cases} \dot{p} = -\mathrm{l}g_2 p - l[g_2 lx + f(x) + g_1(x)u], \\ \hat{d} = p + lx \end{cases} \tag{2}$$

with $x = [x_1, x_2]^T$, $f(x) = [x_2, \hat{a}(x)]^{\mathrm{T}}$, $g_1 = [0, \hat{b}(x)]^{\mathrm{T}}$,

$g_2 = [1, 0]^{\mathrm{T}}$, where $\hat{a}(x)$ and $\hat{b}(x)$ are two nonlinear uncertain functions approximated by the fuzzy System. d, p, and l represent, respectively, the estimated disturbance, the internal state of the nonlinear observer, and the observer gain.

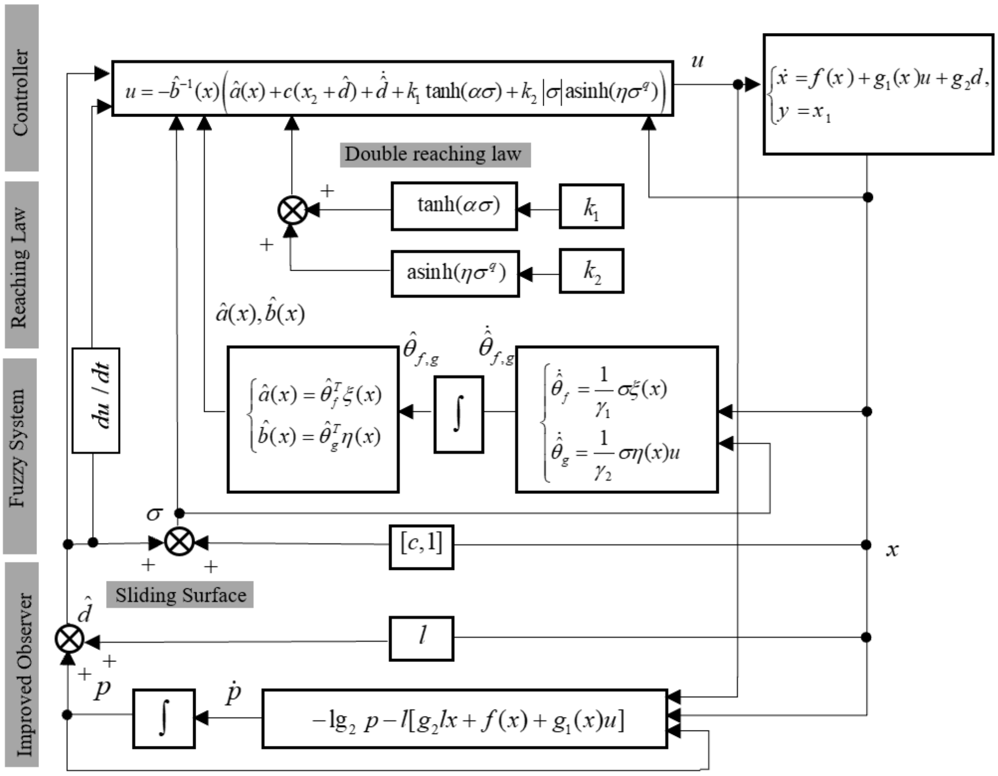

Fig. 1. Diagram illustrating the proposed sliding mode control (SMC).

Assumption 2: The derivatives of the disturbance $d(t)$ in equation (1) are bounded and satisfy the condition $\lim_{t\to\infty} d(t)=0.$

2.2 Fuzzy system

In this paper, the fuzzy system (FS) is adopted because it does not require an explicit mathematical model and offers high computational speed (Ma et al., 2018). Thereby, it has been used to approximate the nonlinear functions a and b of the system (1), By using the principle of FS, the outputs can be represented in the following form (Wang, 1994):

$$\hat{a}(x)=\frac{\Sigma_{i=1}^{m}a^i\left(\prod_{j=1}^{n}\mu_{A_j^i}(x_j)\right)}{\Sigma_{i=1}^{m}\left(\prod_{j=1}^{n}\mu_{A_j^i}(x_j)\right)}=\hat{\theta}_a^T\,\xi(x) \tag{3}$$

$$\hat{b}(x)=\frac{\Sigma_{i=1}^{m}b^i\left(\prod_{j=1}^{n}\mu_{B_j^i}(x_j)\right)}{\Sigma_{i=1}^{m}\left(\prod_{j=1}^{n}\mu_{B_j^i}(x_j)\right)}=\hat{\theta}_b^T\,\eta(x) \tag{4}$$

Let $\Omega(x,\theta_a,\theta_b)$ denote a function defined by

$$w(x,\theta_a,\theta_b)=a(x,t)-\hat{a}(x,\theta_a^*)+ ((b(x,t)-\hat{b}(x,\theta_b^*))u(t) \tag{5}$$

Assumption 3: Ω is a bounded function defined by $w^*=\sup_{t>0}|w(x,\theta_a,\theta_b)|$.

2.3 Continuous reaching law

In this study, a continuous double-reaching approach is employed to minimize chattering and achieve precise tracking performance through adjustment of the switching function. This reaching law is composed of two hyperbolic functions with opposite amplitude characteristics and similar changing rate. The approach utilizes two functions: the inverse hyperbolic sine , *asinh* for fast convergence when the initial sliding surface value σ is distant from equilibrium, and the hyperbolic tangent *tanh* to ensure the sliding surface approaches zero without crossing it as it gets closer. This method is detailed in reference (Tao et al., 2018):

$$\dot{\sigma}=-k_1\tanh(\alpha\sigma)-k_2|\sigma|.\mathrm{asinh}(\eta\sigma^q) \tag{6}$$

with

$$\tanh(\sigma)=\frac{e^{\sigma}-e^{-\sigma}}{e^{\sigma}+e^{-\sigma}} \tag{7}$$

$$\mathrm{asinh}(\sigma)=\ln(\sigma+\sqrt{\sigma^2+1}) \tag{8}$$

where σ is the sliding surface; k_1,k_2,α and η, represent positive tuning parameters, and q denotes the positive power term. For more details about the reaching law, the reader can refer to (Tao et al., 2018).

Lemma 1 (Khalil, 1996): Consider a nonlinear system $\dot{x}=F(x,w)$, which is input-to-state stable (ISS). If the input satisfies $\lim_{t\to\infty} w(t)=0$, then $\lim_{t\to\infty} x(t)=0$.

2.4 Design of the controller and stability analysis

Define the sliding surface σ as follow (Yang et al., 2013):

$$\sigma = x_2 + cx_1 + \hat{d} \tag{9}$$

Theorem 1: Considering system (1) in the presence of uncertainties, mismatched disturbances, and varying system parameters, a new Sliding Mode Controller (SMC) is proposed:

$$u = -\hat{b}^{-1}(x)\begin{pmatrix} \hat{a}(x) + c(x_2 + \hat{d}) + \dot{\hat{d}} + \\ k_1 \tanh(\alpha\sigma) + k_2|\sigma|\operatorname{asinh}(\eta\sigma^q) \end{pmatrix} \tag{10}$$

Suppose that assumptions 1-3 are met, if the sliding surface satisfies $|\sigma| \geq \frac{1}{\alpha}\operatorname{atanh}(\frac{w^* + ce_d^*}{k_1})$, then, the closed-loop system exhibits asymptotic stability.

Proof: Let's define the following Lyapunov function:

$$V = \frac{1}{2}\sigma^2 + \frac{1}{2}\left(\gamma_1 \tilde{\theta}_a^T \tilde{\theta}_a + \gamma_2 \tilde{\theta}_b^T \tilde{\theta}_b\right) \tag{11}$$

where $\gamma_1 > 0, \gamma_2 > 0$

Considering the derivative of the sliding surface σ defined in (9), yields

$$\dot{\sigma} = \dot{x}_2 + c\dot{x}_1 + \dot{\hat{d}} \tag{12}$$

Submitting (1) into (12), it gets

$$\dot{\sigma} = a(x) + b(x)u + c(x_2 + d(t)) + \dot{\hat{d}}(t) \tag{13}$$

Substituting (10) into (13), the following equations can be obtained

$$\begin{aligned} \dot{\sigma} &= a(x) + b(x)u - \hat{a}(x) - c(x_2 + \hat{d}(t)) - k_1\sigma\tanh(\alpha\sigma) \\ &\quad -k_2\sigma|\sigma|\operatorname{asinh}(\eta\sigma^q) - \hat{b}(x)u + c(x_2 + d(t)) \\ &= a(x) - \hat{a}(x) + b(x)u - \hat{b}(x)u + ce_d - k_1\sigma\tanh(\alpha\sigma) \\ &\quad -k_2\sigma|\sigma|\operatorname{asinh}(\eta\sigma^q) \\ &= \theta_a^{*T}\xi(x) - \hat{\theta}_a^T\xi(x) + \theta_b^{*T}\eta(x)u - \hat{\theta}_b^T\eta(x)u + w(x) + \\ &\quad ce_d - k_1\sigma\tanh(\alpha\sigma) - k_2\sigma|\sigma|\operatorname{asinh}(\eta\sigma^q) \end{aligned} \tag{14}$$

Equation (14) can be rewritten as

$$\begin{aligned} \dot{\sigma} &= \tilde{\theta}_a^T\xi(x) + \tilde{\theta}_b^T\eta(x)u + w(x) + ce_d - k_1\sigma\tanh(\alpha\sigma) \\ &\quad -k_2\sigma|\sigma|\operatorname{asinh}(\eta\sigma^q) \end{aligned} \tag{15}$$

where

$$\tilde{\theta}_a = \theta_a^* - \hat{\theta}_a \tag{16}$$

$$\tilde{\theta}_b = \theta_b^* - \hat{\theta}_b \tag{17}$$

Taking the time derivative of the Lyapunov function defined in Equation (11), yields

$$\dot{V} = \sigma\dot{\sigma} + \gamma_1\tilde{\theta}_a^T\dot{\hat{\theta}}_a + \gamma_2\tilde{\theta}_b^T\dot{\hat{\theta}}_b \tag{18}$$

Then, by substituting (15) into (18), the following equations can be derived

$$\begin{aligned} \dot{V} &= \sigma\begin{pmatrix} \tilde{\theta}_a^T\xi(x) + \tilde{\theta}_b^T\eta(x)u + w(x) + ce_d - \\ k_1\sigma\tanh(\alpha\sigma) - k_2\sigma|\sigma|\operatorname{asinh}(\eta\sigma^q) \end{pmatrix} \\ &\quad -\gamma_1\tilde{\theta}_a^T\dot{\hat{\theta}}_a - \gamma_2\tilde{\theta}_b^T\dot{\hat{\theta}}_b \end{aligned} \tag{19}$$

Hence, the adaptive rules are designed as follows

$$\dot{\hat{\theta}}_a = \frac{1}{\gamma_1}\sigma\xi(x) \tag{20}$$

$$\dot{\hat{\theta}}_b = \frac{1}{\gamma_2}\sigma\eta(x)u \tag{21}$$

Substituting Equations (20) and (21) into Equation (19) gives

$$\begin{aligned} \dot{V} &= \sigma w + \sigma ce_d - k_1\sigma\tanh(\alpha\sigma) - k_2\sigma|\sigma|\operatorname{asinh}(\eta\sigma^q) \\ &\leq |\sigma|(w^* + ce_d^*) - k_1\sigma\tanh(\alpha\sigma) - \\ &\quad k_2\sigma|\sigma|\operatorname{asinh}(\eta\sigma^q) \\ &= -\left(k_1\tanh(\alpha\sigma)sign(\sigma) - (w^* + ce_d^*)\right)|\sigma| - \\ &\quad k_2\sigma|\sigma|\operatorname{asinh}(\eta\sigma^q) \\ &= -\left(k_1\tanh(\alpha|\sigma|) - (w^* + ce_d^*)\right)|\sigma| - \\ &\quad k_2\sigma|\sigma|\operatorname{asinh}(\eta\sigma^q) \end{aligned} \tag{22}$$

From (22), it can be found that $k_2\sigma|\sigma|\operatorname{asinh}(\eta\sigma^q)$ is always ≥ 0, to ensure system stability, it must satisfy that:

$$k_1\tanh(\alpha|\sigma|) \geq (w^* + ce_d^*) \tag{23}$$

And it leads to

$$|\sigma| \geq \frac{1}{\alpha}\operatorname{atanh}(\frac{w^* + ce_d^*}{k_1}) \tag{24}$$

This means that $\dot{V} \leq 0$ is obtained when the sliding surface $|\sigma|$ satisfies $|\sigma| \geq \frac{1}{\alpha}\operatorname{atanh}(\frac{w^* + ce_d^*}{k_1})$. Then, the sliding surface σ converges to the bound of $\frac{1}{\alpha}\operatorname{atanh}(\frac{w^* + ce_d^*}{k_1})$ from the initial value σ_0, i.e. the bound of system steady state error is $|\sigma| \leq \frac{1}{\alpha}\operatorname{atanh}(\frac{w^* + ce_d^*}{k_1})$ when the system has a bounded disturbances estimation errorWith this result . w^* and e_d^* obtained in (22), the system states will attain the sliding surface $\sigma = 0$ within a finite time, implying that:

$$\dot{x}_1 = -cx_1 + e_d \tag{25}$$

Therefore, it follows from Lemma 5.5 (Khalil, 1996) that (25) satisfies the conditions for Input-to-State Stability (ISS).

From Lemma 1, one can see that the system states satisfy $\lim_{t\to\infty} e_d(t) = 0$ and $\lim_{t\to\infty} x_1(t) = 0$. Which implies that the system states converge to equilibrium point along the sliding surface σ. For more detail about the reaching law and the initial value of the sliding surface σ_0 the reader can refer to (Tao et al., 2018), the resulting block diagram in Fig. 1 summarizes the proposed controller.

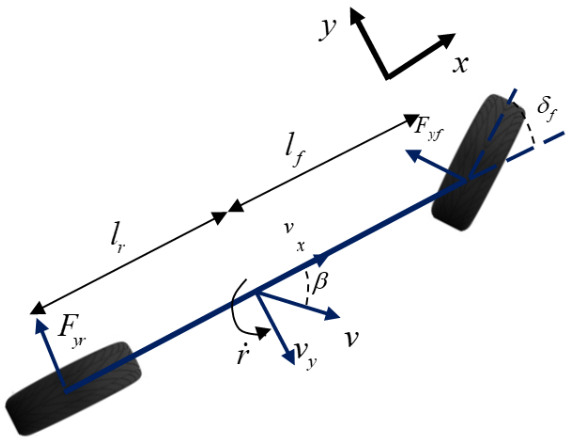

Fig. 2. Schematic of the vehicle lateral dynamics model.

3. APPLICATION TO THE AUTONOMOUS VEHICLE

To validate the proposed SMC developed above, this section aims to apply it to autonomous vehicles.

3.1 Vehicle Dynamics model

In this research, a two degrees of freedom (2DoF) model is used to characterize the vehicle's lateral dynamics, as illustrated in Fig. 2. This model effectively captures the essential behaviors and interactions influencing lateral motion. The equations governing the dynamics of the vehicle model in the yaw plane, as outlined in (Tagne et al., 2015; Rajamani., 2011), can be expressed as follows (vehicle parameters are detailed in Table 1):

$$\begin{cases} \dot{\beta} = -\dfrac{\mu(C_f + C_r)}{mV_x}\beta - \left(1 + \dfrac{\mu(L_f C_f - L_r C_r)}{mV_x^2}\right)\dot{r} + \dfrac{\mu C_f}{mV_x}\delta_f \\ \ddot{r} = -\dfrac{\mu(L_f C_f - L_r C_r)}{I_z}\beta - \dfrac{\mu(L_f^2 C_f + L_r^2 C_r)}{I_z V_x}\dot{r} + \dfrac{\mu L_f C_f}{I_z}\delta_f \\ \dot{x}_2 = -\dfrac{\mu(C_f + C_r)}{m}\beta - \dfrac{\mu(l_f C_f - l_r C_r)}{mv_x}\dot{r} + \dfrac{\mu C_f}{m}\delta_f - V_x^2\rho \\ \dot{x}_1 = x_2 + d \end{cases} \tag{26}$$

The Equation of the lateral error and its derivative can be written as

$$\begin{cases} \dot{x} = f(x) + g_1 u + g_2\rho + g_3 d, \\ y = x_1 \end{cases} \tag{27}$$

where $x = [x_1, x_2]^T$, $f(x) = [x_2, a]^T$, $g_1 = [0, b_1]^T$, $g_2 = [0, b_2]^T$, $g_3 = [1, 0]^T$, $u = \delta_f$.

3.2 Application of the proposed controller to the lateral control

After presenting our SMC controller, it will be applied to enhance the transient tracking performance in the lateral control of autonomous vehicles. This includes handling speed/curvature variations, tire nonlinearities, mismatched disturbances, and system uncertainties.

Choosing the sliding surface σ as (9) and based on the proposed controller, i.e. theorem 1, the control input is obtained as follows:

$$\delta_f = -\hat{b}_1^{-1}(x)\begin{pmatrix} \hat{a}(x) + b_2\rho + c(x_2 + \hat{d}) + \dot{\hat{d}} + \\ k_1 \tanh(\alpha\sigma) + k_2|\sigma| \operatorname{asinh}(\eta\sigma^q) \end{pmatrix} \tag{28}$$

where ρ represents the road curvature of the reference path.

The equations of the improved DOB are obtained as follows:

$$\begin{cases} \dot{p} = -lg_3 p - l[g_3 lx + f(x) + g_1(x)u + g_2\rho], \\ \hat{d} = p + lx, \end{cases} \tag{29}$$

where $x = [x_1, x_2]^T$, $f(x) = [x_2, \hat{a}]^T$, $g_1 = [0, \hat{b}_1]^T$, $g_2 = [0, b_2]^T$, $g_3 = [1, 0]^T$.

To show the advantage of the addition of the fuzzy system to our controller, the fuzzy system has been removed from the controller proposed (theorem 1) and the disturbance observer (29), and then, the control law (28) is modified as

$$\delta_f = -b_1^{-1}(x)\begin{pmatrix} a(x) + b_2\rho + c(x_2 + \hat{d}) + \\ \dot{\hat{d}} + k_1 \tanh(\alpha\sigma) + k_2|\sigma| \operatorname{asinh}(\eta\sigma^q) \end{pmatrix} \tag{30}$$

And the equations of the standard DOB are defined as follow:

$$\begin{cases} \dot{p} = -lg_3 p - l[g_3 lx + f(x) + g_1(x)u + g_2\rho], \\ \hat{d} = p + lx, \end{cases} \tag{31}$$

where $x = [x_1, x_2]^T$, $f(x) = [x_2, a]^T$, $g_1 = [0, b_1]^T$, $g_2 = [0, b_2]^T$, $g_3 = [1, 0]^T$.

Remark 1: the proof of the stability of the controller (28), follow the same steps mentioned in section, except that the condition of the stability $k_1 \tanh(\alpha|\sigma|) \geq (w^* + ce_d^*)$, must be changed by $k_1 \tanh(\alpha|\sigma|) \geq ce_d^*$.

3.3 Sliding Mode Controller based on Super-twisting algorithm

The algorithm of Super-twisting (ST) is a two-order sliding mode control. The ST is one of the effective algorithms against the perturbations, and it has great capacities to remove chattering, which renders the controller robust, continuous, and smooth. This algorithm is extensively used in complex industrial systems and in recent works like (Wogi et al., 2024; Xu et al., 2023; Zang et al., 2024). In the following, the Super-twisting algorithm is demonstrated and its application through the controller developed in (Tagn et al., 2016) is shown, in which it was applied to the lateral control of autonomous vehicle.

The application of the SMC Super-twisting to the lateral control is defined as:

$$\delta_f = -b_1^{-1}(x)\left(a(x)+b_2\rho+cx_2\right)+\alpha_1|\sigma|^{\frac{1}{2}}sign(\sigma) \\ +\alpha_2\int sign(\sigma) \tag{32}$$

The readers can also refer to (Tagn et al., 2016) for more details about the algorithm of ST and its application.

3.4 Conventional sliding mode controller

In the following, the conventional SMC to the lateral control of autonomous vehicle is applied:

$$\delta_f = -b_1^{-1}(x)\left(a(x)+b_2\rho+cx_2+ksign(\sigma)\right) \tag{33}$$

where k is a positive constant.

4. RESULTS AND DISCUSSION

This section presents three simulation cases, implemented based on Matlab/Simulink and Carsim. The latter is used to obtain the road's curvature and longitudinal speed. For these test cases, different road adhesion coefficients are adopted to verify the performances and the robustness of the proposed controller, thus the disturbances and the system uncertainties are already included in the simulations. The objective is to make the vehicle follow the reference path with ensured safety and stability. In all cases of simulation, the vehicle runs at a high and variable speed: $v_x \in [50,155]$ *km/h* and with curvature of road $\rho \in [-0.03, 0.05]$ m^{-1}, which includes very sharp turns. To highlight the superiority of our controller, the SMC based on the Super-twisting algorithm is utilized to conduct a comparative simulation. The reason behind choosing SMC super-twisting is its robustness, capable of achieving very low errors, and its widespread use in recent works, as mentioned previously.

In all simulation scenarios, the proposed controller is named as AFSMC-DOB, i.e. adaptive fuzzy sliding mode control based on disturbance observer. However, to show the advantage of the addition of the fuzzy system to the proposed controller, the controller ASMC-DOB is included in the comparative simulation, however, this controller has the same structure of the proposed controller except that it has not the fuzzy system. In addition, the conventional SMC is used in the first test to shows the improvements made by the proposed controller. It is noted that the conventional SMC is utilized only in the first test because the results obtained by this controller are unacceptable.

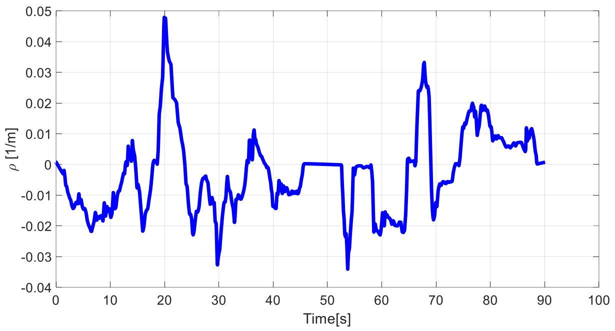

Fig. 3. Road curvature of the reference path.

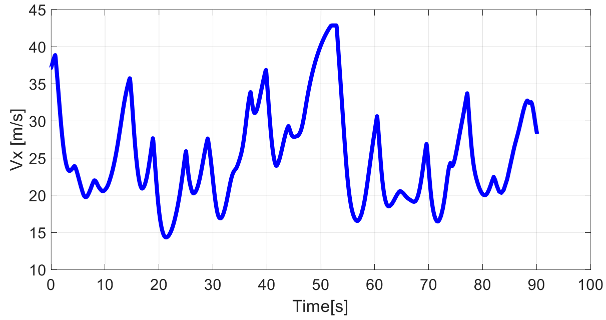

Fig. 4. Longitudinal Speed.

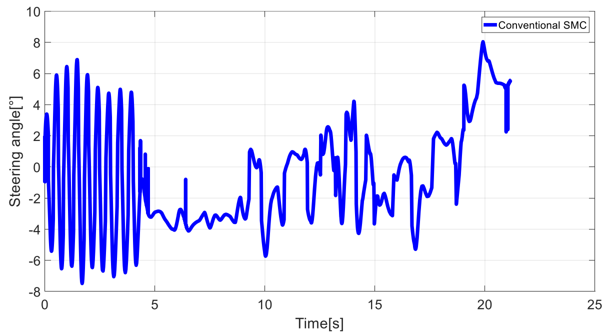

Fig. 5. The control input result with 13% of uncertainties and $\mu \in [0.8,1]$.

Accurately determining tire cornering stiffness is indeed challenging. This parameter is highly sensitive to factors such as road conditions, vertical loads, and wheel camber. Similarly, the vehicle's mass can vary or be inaccurately estimated due to changes in passenger count, fuel levels, and other related factors (Tagne et al., 2016). To address these uncertainties, we have relied on rates commonly reported in the literature, which account for realistic variations in these parameters under typical operating conditions. Specifically, our choices were informed by studies such as (Nguyen et al., 2020; El Hajjami et al., 2021; Tagne et al., 2016), which provide well-documented ranges for these uncertainties. This approach ensures that the proposed methods are tested against conditions that reflect practical scenarios.

The perturbations are introduced into three main levels: law, middle and high, in which the vehicle runs at high speed in extreme conditions and under different road friction conditions (Nielsen and Kiencke, 2005). It is noted that the uncertainties are included gradually in each test, i.e., in each level, however, the mismatched disturbances are not included in the two first tests, since the goal is to show the behavior of controllers against the uncertainties. The control parameters for the control strategies and the vehicle parameters used in the simulation are given in table 1 and table 2, respectively.

Assumption 4 : It is assumed that the estimated disturbance $\hat{d}$ varies very slowly over time, such that its time derivative $\dot{\hat{d}}$ can be approximated as zero.

*Remark 2***:** because $b_1(x)$ has an almost constant value, it can be determined using an "if-then" condition based on x at the beginning of the simulation or keep the nominal value of $b_1(x)$ as it is, in our case we keep the nominal value of $b_1(x)$ as it is.

Remark 3: Many researches have been carried on the vehicle lateral control like (Tagn et al., 2016; Hu et al., 2018; Lin et al., 2023). Although most studies assume that the speed is constant and that the highest speed mentioned in the literature does not surpass 120 km/h, the driving in our work occurs at high speed until 155 km/h as well as it varies very quickly (see Fig. 4).

4.1 First Test: Law Nonlinear Situation

In the first simulation, the controlled vehicle moves on road with the tire-road friction coefficient: $\mu \in [0.8, 1]$, and the rate of the uncertainties for the mass and the cornering stiffness are set as 15% of the normal value: $m = m + 15\%$, $c_f = c_f + 15\%$, $c_r = c_r + 15\%$.

The control input and the lateral error results of the conventional SMC are presented in Fig. 5 and Fig. 6 respectively. It can be observed that the steering angle is not kept within a reasonable range where it provides a lot of chattering, and has not a similar varying trend compared with the curvature of the road of the reference path (see Fig. 3).

Fig. 6 shows that the lateral error increases over time. It is noted that the conventional SMC did not complete the simulation and it stops after 21s, due to its low performances against the uncertainties, however, the simulation must finish at the 90s as shown in the Fig. 7.

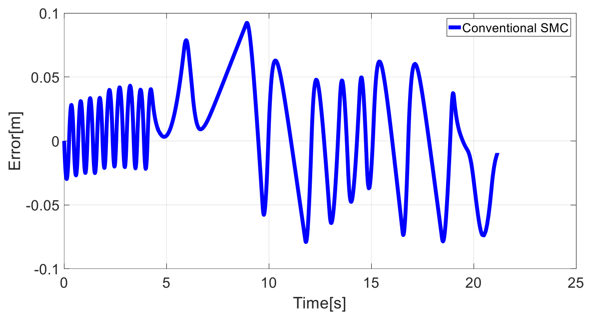

Fig. 6. Lateral error with 13% of uncertainties and $\mu \in [0.8, 1]$.

It is noted that a 13% rate of uncertainties was applied to the mass and cornering stiffness of the vehicle controlled by the conventional SMC, while a 15% rate was used for the rest of this test.

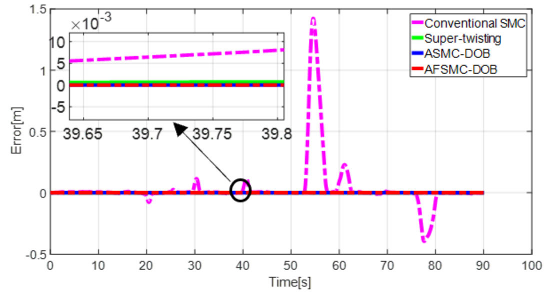

Fig. 7. Lateral error with 15% of uncertainties and $\mu \in [0.8, 1]$.

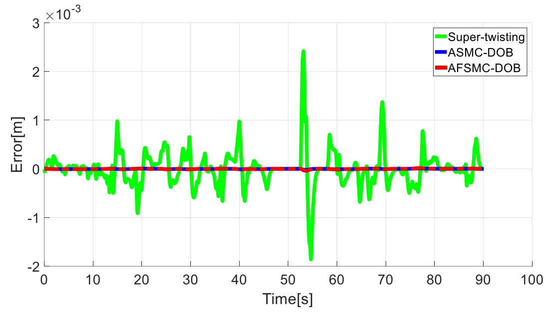

Fig. 8. Lateral error with 15% of uncertainties and $\mu \in [0.8, 1]$.

The obtained results achieved with conventional SMC are unacceptable, for this, it will be necessary to replace the function “sign” by “sat”. The lateral error result is shown in Fig. 7 One can see that the lateral error given by the conventional SMC is improved compared to the Fig. 6, but it converged to zero when the vehicle runs at middle speed, and since the vehicle begins to increase the speed the lateral error also increases and reaches about 1.4 m, causing a great danger to the vehicle stability.

Table 1. Vehicle Parameters

Index	*Variable*	*Val*	*U*
m	mass	(1421)	[kg]
V_y	Lateral Speed	-	[m/s]
I_z	yaw moment	(2570)	[kg.m^2]
l_f , l_r	Front/rear axle to center of gravity distance	(1.20, 1.50)	[m]
δ_f	Steering angle	-	[rad]
F_{yf}, F_{yr}	Lateral tire forces	-	[rad]
B	Sideslip Angle	-	[rad]
r	Yaw angle	-	[rad]
v_x	Longitudinal velocity range	[19-45]	[m/s]
C_f , C_r	Cornering stiffness	(170500,137840)	[N/rad]
μ	Friction coefficient	[0-1]	-
d	Disturbance	-	-

In Fig. 8, the conventional SMC has been removed to be able to compare the SMC Super-twisting and the proposed controller. From this Figure, one can observe that the three controllers: Super-twisting, ASMC-DOB, AFSMC-DOB can stabilize the path following errors, but for the ASMC-DOB and AFSMC-DOB case, the transient performances of the lateral error responses are apparently improved. In the rapid variations of parameters i.e. in the sharp turn ($t \in [52, 58]$), the SMC Super-twisting causing a big peak and the lateral error reach about 2x10^{-3} m, however, the AFSMC-DOB and ASMC-DOB showed great robustness.

This quantitatively shows the superior transient performance improvement of the proposed controller AFSMC-DOB compared to the Super-twisting.

In addition, Fig. 8 displays the advantage of the proposed controller at the level of the robustness compared with Super-twisting is very large.

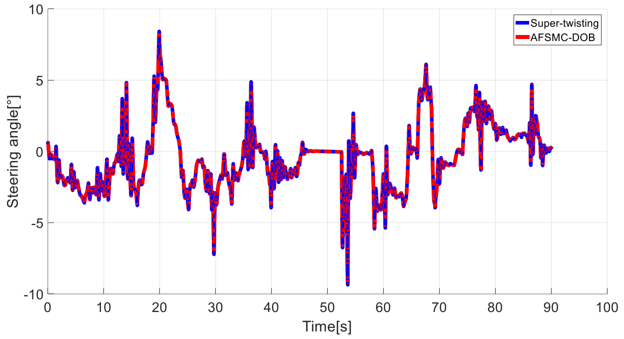

Fig. 9. The control inputs results: Super-twisting and AFSMC-DOB.

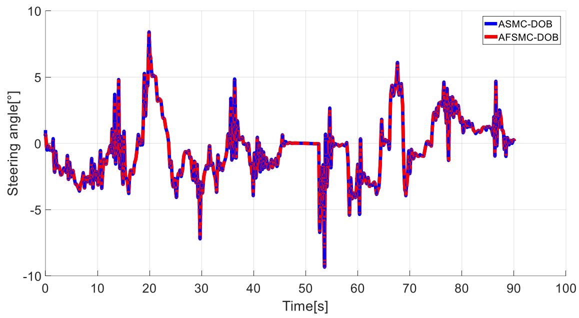

Fig. 10. The control inputs results: ASMC-DOB and AFSMC-DOB.

The steering angles is shown in Fig. 9 and Fig.10 one can see that the steering angles provided by the three controllers: Super-twisting, ASMC-DOB and AFSMC-DOB are controlled in reasonable region where they have an analogous variation trend compared to the curvature of the reference path.

The path following trajectory results are depicted in Fig. 11. It is found that the three controllers Super-twisting, ASMC-DOB and AFSMC-DOB controllers can effectively increase the accuracy of path tracking compared to the conventional SMC and this is very clear in sharp turns. Through the comparison, by using the AFSMC-DOB, it can be observed that the lateral error has less oscillations, smaller shocks, and can be stabilized faster in a considerably short time compared with the SMC Super-twisting and the conventional SMC demonstrating the effectiveness of the proposed control strategy.

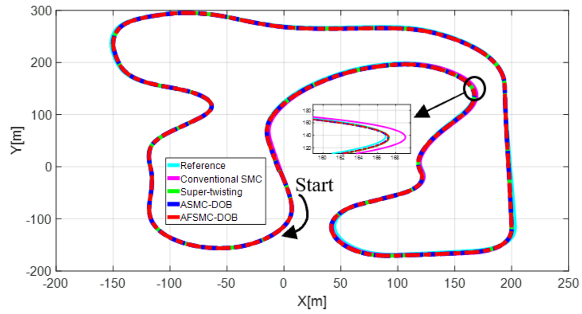

Fig. 11. The path following trajectory results under 15% of uncertainties and $\mu \in [0.8, 1]$.

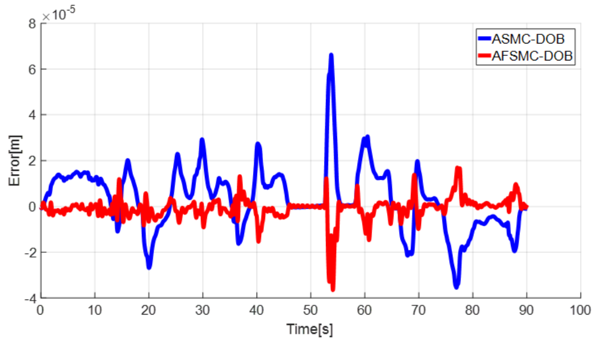

Fig. 12. Lateral error with 15% of uncertainties and $\mu = 0.4$.

To compare the two proposed controllers, ASMC-DOB and AFSMC-DOB, in terms of lateral error, we selected a high tire-road friction coefficient $\mu = 0.4$ and maintained the same rate of uncertainties at 15%. As observed in Fig. 12, the AFSMC-DOB significantly reduces the lateral error compared to ASMC-DOB, greatly enhancing vehicle stability and safety.

4.2 Second Test: Middle Nonlinear Situation

In this second scenario, the rate of uncertainties in the cornering stiffness and vehicle mass is increased. As a result, the vehicle's behavior becomes non-linear. The uncertainties are set as 30% of the normal value: $c_f = c_f + 30\%$, $c_r = c_r + 30\%$, $m = m + 30\%$, and the road frictions is $\mu = 0.1$.

The path following trajectory results are shown in Fig. 13. It is found that the two controllers ASMC-DOB and AFSMC-DOB controllers can effectively enhance the accuracy of path tracking compared to the SMC Super-twisting, as clearly demonstrated in the applied zoom. The lateral error results are shown in Fig. 14 and Fig. 15. It is showed that the SMC Super-twisting is more sensitive to the uncertainties and the variation of parameters (Curvature and Speed) compared to the ASMC-DOB and the AFSMC-DOB.

From Fig. 15, it can be found that the AFSMC-DOB adapts effectively against the perturbations and it can minimize considerably the lateral error despite the high rate of the uncertainties, the high speed and the sharp turns. Moreover, it converges the lateral error to zero, but with the ASMC-DOB, the error converges to small value but non-zero.

Table 2. Controllers' parameters

Controller	*Parameters*
Conventional SMC	$c=5, k=3$
SMC Super-twisting	$c=5, \alpha_1=2, \alpha_2=8$
ASMC-DOB	$c=5, k_1=10^4, k_2=10^4, \alpha=15, \eta=10, q=9, l=[6,0]$
AFSMC-DOB	$c=5, k_1=10^4, k_2=10^4, \alpha=15, \eta=10, q=9, \gamma_1=0.05, l=[6,0]$

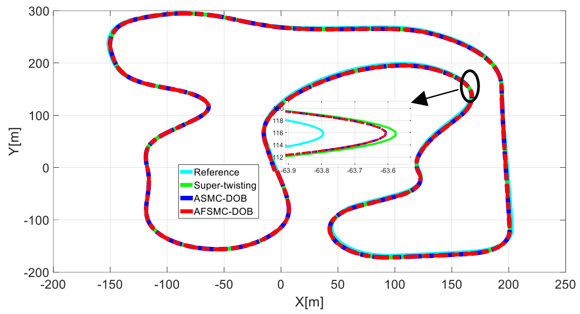

Fig. 13. The path following trajectory results with 30% of uncertainties and $\mu=0.1$.

The results of the two tests demonstrated that the AFSMC-DOB outperforms the SMC Super-Twisting and ASMC-DOB controllers. In particular, the AFSMC-DOB maintained good performance in the second test, despite an increase in the uncertainties rate by up to 30%. This indicates that the proposed controller adapts more effectively to uncertainties, with robustness that scales proportionally to the perturbations encountered.

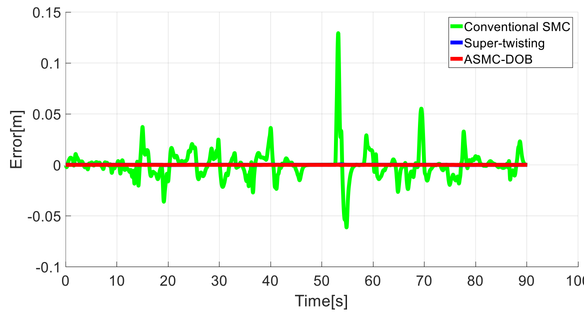

Fig. 14. Lateral error with 30% of uncertainties and $\mu=0.1$.

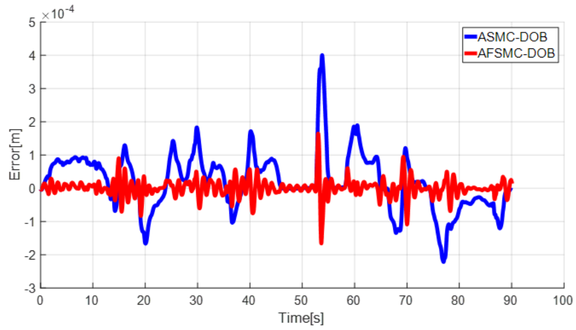

Fig. 15. Lateral error with 30% of uncertainties and $\mu=0.1$.

Therefore, this obtained result shows us that the addition of the fuzzy system allows to our controller to obtain an intelligent behavior against the uncertainties. It is noted that the lateral errors provided by the SMC Super-twisting are very increased compared with the first test. Thus, one can conclude that the lateral control using AFSMC-DOB has retained advantages of fuzzy system and SMC, and is more accurate and much faster than using the SMC Super-twisting, which is ultimately of great advantage for enhancing the vehicle safety, stability, and comfort.

Remark 4: the proposed controller is a type of controller most demanded In the field of control, due to its high robustness against perturbations such as uncertainties, the sharp turns…etc, therefore, the AFSMC-DOB can be applied to several systems (aerospace engineering, aircraft, tractors, MAGNETV Suspension, missiles and satellites .... etc.).

4.3 Third test: High Nonlinear Situation

This test involves the inclusion of mismatched disturbances, causing the vehicle's behavior to become highly non-linear. The uncertainties are set as 30% of the normal value: $c_f = c_f + 30\%$, $c_r = c_r + 30\%$, $m = m + 30\%$, the road friction value is: $\mu = 0.1$, and the mismatched disturbances are set as : $d \in [-1,1]$.

The lateral error results are shown in Fig. 16. From this figure, one can see that both controllers: ASMC-DOB and AFSMC-DOB can stabilize the path following errors. However for the SMC Super-twisting case, the transient performances of lateral error responses are apparently unacceptable, and it has an analogous variation trend compared to the mismatched disturbance (see Fig. 17).

In addition, it cannot converge the lateral error to 0 and exceeds 0.3 m, which means that the SMC Super-twisting cannot handle the mismatched disturbance. However, Fig. 17 shows that the disturbance can be accurately estimated by the improved observer (DOB-FS), as shown in the zoom applied. The mismatched disturbance estimation and the disturbances estimation error results are shown in Fig. 17 and Fig. 18, respectively. From Fig. 17, it can be found that the both observers, i.e. the improved observer: DOB-FS and the standard observer: DOB, can give an acceptable result. Fig. 18 demonstrates that the improved observer :DOB-FS, produces a smaller error compared to the standard observer : DOB. Table 3 summarizes the comparison between the control strategies.

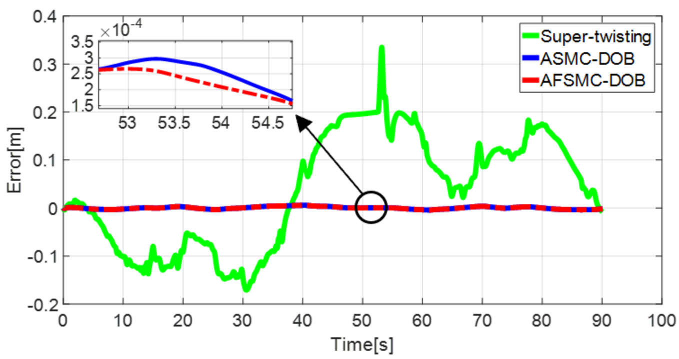

Fig. 16. Lateral error with 30% of uncertainties, mismatched disturbance $d \in [-1,1]$ and $\mu=0.1$.

Table 3. Comparison Between Control Strategies

Strategy	*Pros*	*Cons*
Conventional SMC	• Simple control strategy	• Sensitive to the uncertainty parameters • Sensitive to variations of speed and curvature (parameter variations) • Chattering
SMC Super-twisting	• Relatively simple control strategy • Robust against uncertainties with medium level. • eliminate the chattering	• Sensitive to the mismatched disturbances. • Sensitive to variations of speed and curvature (parameter variations)
Proposed controller AFSMC-DOB	• Robust against variations of parameters (curvature and speed). • Robust against uncertainties with very high level. • Robust against the mismatched disturbances. • Its robustness is proportional with the perturbations encountered. • Stability Robust • eliminate the chattering	----

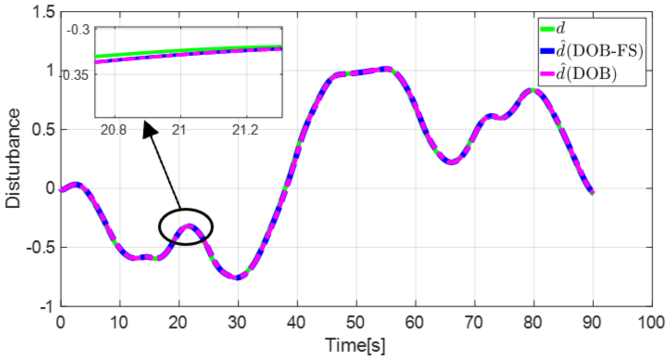

Fig. 17. Mismatched disturbance estimation.

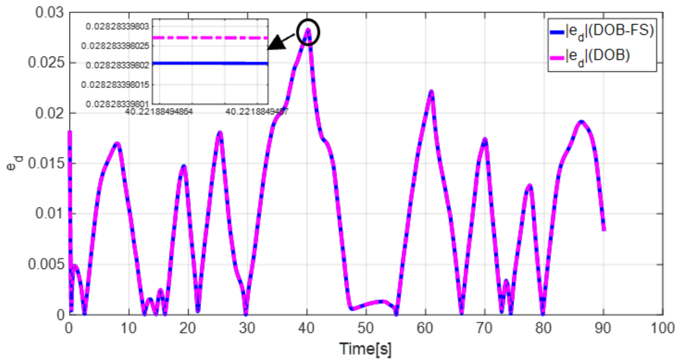

Fig. 18. Disturbance estimation error.

5. CONCLUSION

This paper presents a new control strategy for the lateral control of autonomous vehicles. Several tests and scenarios were conducted on the developed controller, clearly demonstrating the expected outcomes. The proposed AFSMC-DOB controller (according to Theorem 1) combines Sliding Mode Control (SMC) with a Fuzzy System and a Double Reaching Law, providing complementary control and superior performance against uncertainties and parametric variations.

Furthermore, the enhanced disturbance observer accurately estimates mismatched disturbances, effectively addressing chattering issues and overcoming the drawbacks of conventional SMC. Compared to the conventional SMC and the Super-Twisting SMC control, the path-following results in terms of lateral control demonstrate that the proposed SMC significantly enhances vehicle stability and safety in critical situations, such as collision avoidance.

In upcoming research, the objective is to compare the proposed control strategy with alternative methods, including H∞ and LQR.

REFERENCES

Akermi, K., Chouraqui, S., & Boudaa, B. (2018). Novel SMC control design for path following of autonomous vehicles with uncertainties and mismatched disturbances. *International Journal of Dynamics and Control*, pp. 1-15.

Chen, Bor-Sen, Hao-Ting Liu, and Ruei-Syuan Wu. (2024). Robust H∞ Fault-tolerant Observer-based PID Path Tracking Control of Autonomous Ground Vehicle with Control Saturation. *IEEE Open Journal of Vehicular Technology.*

Chen, Jiancheng, et al. (2020). Path following control of autonomous four-wheel-independent-drive electric vehicles via second-order sliding mode and nonlinear disturbance observer techniques. *IEEE Transactions on Industrial Electronics*, 68(3), 2460-2469.

Chen, W. (2003). Dynamic Inversion Control of Missiles. Vol. 26, 1, 161-166.

Cheng, Shuo, et al. (2020). Model-predictive-control-based path tracking controller of autonomous vehicle considering parametric uncertainties and velocity-varying. *IEEE Transactions on Industrial Electronics*, 68(9), 8698-8707.

El Hajjami, L., Mellouli, E. M., and Berrada, M. (2021). Robust Adaptive Non-Singular Fast Terminal Sliding-Mode Lateral Control for an Uncertain Ego Vehicle at the Lane-Change Maneuver Subjected to Abrupt Change. *International Journal of Dynamics and Control*, pp. 1-18.

Fu, Rui, et al. (2023). Lateral Stability Control of Buses: A Framework Considering the Steering Hysteresis Response Using Interleaved Predictive Control. *IEEE Transactions on Vehicular Technology.*

Hu, C., Wang, R., Yan, F., Huang, Y., Wang, H., & Wei, C. (2018). Differential steering based yaw stabilization using ISMC for independently actuated electric vehicles. *IEEE Transactions on Intelligent Transportation Systems*, 19(2), 627-638.

Jin, Long, et al. (2024). Physical-informed neural network for MPC-based trajectory tracking of vehicles with noise considered. *IEEE Transactions on Intelligent Vehicles*.

Khalil, H.K. (1996). Nonlinear Systems. Upper Saddle River, *NJ: Prentice-Hall*.

Liang, Y., Li, Y., Khajepour, A., and Zheng, L. (2021). Holistic adaptive multimodel predictive control for the path following of 4WID autonomous vehicles. *IEEE Transactions on Vehicular Technology*, 70(1), 69-81. doi: 10.1109/TVT.2020.3046052.

Lin, F., Wang, X., Qian, C., Zhao, Y., & Wu, J. (2023). Coordinated longitudinal and lateral motion control for distributed drive electric vehicles with mechanical elastic wheels. *IEEE Transactions on Transportation Electrification*.

Lukassek, Markus, et al. (2024). Model predictive path-following control for truck–trailer systems with specific guidance points—design and experimental validation. *Mechatronics*, 100, 103190.

Ma, X., Kin, P., Zhao, J. and Xie, Z. (2018). Cornering stability control for vehicles with active front steering system using T-S fuzzy based sliding mode control strategy. *Mechanical Systems and Signal Processing*.

Meng, Dele, et al. (2024). Real-Time High-Precision Nonlinear Tracking Control of Autonomous Vehicles Using Fast Iterative Model Predictive Control. *IEEE Transactions on Intelligent Vehicles.*

Muraleedharan, A., Okuda, H., and Suzuki, T. (2022). Real-time implementation of randomized model predictive control for autonomous driving. *IEEE Transactions on Intelligent Vehicles,* 7(1), 11-20. doi: 10.1109/TIV.2021.3062730.

Nguyen, A.-T., Rath, J., Guerra, T.-M., et al. (2020). Robust Set-Invariance Based Fuzzy Output Tracking Control for Vehicle Autonomous Driving Under Uncertain Lateral Forces and Steering Constraints. *IEEE Transactions on Intelligent Transportation Systems*, Vol. 22, No. 9, pp. 5849-5860.

Nguyen, Nhu Toan, et al. (2022). Observer-based lateral motion control of an autonomous vehicle via Takagi-Sugeno fuzzy system. In Name(s) of editor(s) (ed.), *International Conference on Green Technology and Sustainable Development*. Cham: Springer International Publishing.

Nielsen, L., Kiencke U. (2005). Automotive Control Systems. *Springer-Verlag*.

Pyun, Beomjoon, Hyungjeen Choi, and Dohyun Jung. (2024). Development of a real-time autonomous driving lateral control algorithm for an articulated bus using a model predictive control algorithm. *Journal of Mechanical Science and Technology*, 38(2), 901-914.

Rajamani, R. (2011). Vehicle Dynamics and Control. *Springer Science & Business Media*.

Sun, H., Zhao, H., Huang, K. and Zhen, S. (2018). A New Approach for Vehicle Lateral Velocity and Yaw Rate Control with Uncertainty. *Asian Journal of Control*, 20(1), 216-227.

Tagne, G., Talj, R. and Charara, A. (2016). Design and Comparison of Robust Nonlinear Controllers for the Lateral Dynamics of Intelligent Vehicles. *IEEE Transactions on Intelligent Transportation Systems*, 17(3), 796-809.

Tagne, G., Talj, R., and Charara, A. (2015). Design of passivity-based controllers for lateral dynamics of intelligent vehicles. In Name(s) of editor(s) (ed.), *Proceedings of IEEE Intelligent Vehicles Symposium*, pp. 1044-1049.

Tao, L., Chen, Q., Nan, Y. and Wu, C. (2018). Double Hyperbolic Reaching Law with Chattering-Free and Fast Convergence. Vol. 6, pp. 27717-27725.

Wang, L.X. (1994). Adaptive Fuzzy Systems and Control, Design and stability analysis.

Wogi, Lelisa, Marcin Morawiec, and Tadele Ayana. (2024). Sensorless Control of Induction Motor Based on Super-Twisting Sliding Mode Observer With Speed Convergence Improvement. *IEEE Access*.

Xu, D., Shi, Y. and Ji, Z. (2018). Model-Free Adaptive Discrete-Time Integral Sliding-Mode-Constrained-Control for Autonomous 4WMV Parking Systems. *IEEE Transactions on Industrial Electronics*, 65(1), 834-843.

Xu, Jing, Yugang Niu, and Peng Shi. (2023). Adaptive multi-input super twisting control for a quadrotor: Singular perturbation approach. *IEEE Transactions on Industrial Electronics*, 71(5), 5195-5204.

Yang, J., Li, S., Member, S. and Yu, X. (2013). Sliding-Mode Control for Systems With Mismatched Uncertainties via a Disturbance Observer. Vol. 60, 1, 160-169.

Yang, Wenhao, Shihong Ding, and Chen Ding. (2024). Fast supertwisting sliding mode control with antipeaking extended state observer for path-tracking of unmanned agricultural vehicles. *IEEE Transactions on Industrial Electronics.*

Zhang, Junda, et al. (2023). Event-Triggered Adaptive Fuzzy Approach-based Lateral Motion Control for Autonomous Vehicles. *IEEE Transactions on Intelligent Vehicles*.

Zhang, Shijun, Shuhong Cheng, and Zhenlin Jin. (2024). Variable Trajectory Impedance: A Super-Twisting Sliding Mode Control Method for Mobile Manipulator Based on Identification Model. *IEEE Transactions on Industrial Electronics.*